Icarus 296 (2017) 49–58

Contents lists available at ScienceDirect

Icarus

journal homepage: www.elsevier.com/locate/icarus

Abiotic versus biotic iron mineral transformation studied by a miniaturized backscattering Mössbauer spectrometer (MIMOS II), X-ray diffraction and Raman spectroscopy

C. Markovski[a], J.M. Byrne[b], E. Lalla[c,d,*], A.D. Lozano-Gorrín[e], G. Klingelhöfer[a], F. Rull[f], A. Kappler[b], T. Hoffmann[a], C. Schröder[g]

[a] Institut für Anorganische Chemie und Analytische Chemie, Johannes Gutenberg Universität Mainz, Staudinger Weg 9, 55128 Mainz, Germany
[b] Geomicrobiology, Center for Applied Geoscience, Eberhard Karls Universität Tübingen, Sigwartstrasse 10, 72076 Tübingen, Germany
[c] Centre for research in earth and space science, York University, Petrie Science Building, 4700 Keele St, Toronto, M3J 1P3, Ontario, Canada
[d] Austrian Space Forum, Sillufer 3a, Innsbruck, 6020, Austria
[e] Departamento de Física, Universidad de La Laguna, 38200 San Cristóbal de La Laguna, Santa Cruz de Tenerife, Spain
[f] Unidad Asociada UVa-CSIC a traves del Centro de Astrobiologia Edificio INDITI, Parque Tecnologico de Boecillo, Parcela 203, E-47151 Boecillo (Valladolid), Spain
[g] Biological and Environmental Sciences, Faculty of Natural Sciences, University of Stirling, Stirling FK9 4LA, Scotland, UK

ARTICLE INFO

Article history:
Received 1 December 2016
Revised 23 May 2017
Accepted 24 May 2017
Available online 25 May 2017

Keywords:
Bio-magnetite
Mössbauer spectroscopy
Raman spectroscopy
Iron oxides

ABSTRACT

Searching for biomarkers or signatures of microbial transformations of minerals is a critical aspect for determining how life evolved on Earth, and whether or not life may have existed in other planets, including Mars. In order to solve such questions, several missions to Mars have sought to determine the geochemistry and mineralogy on the Martian surface. This research includes the two miniaturized Mössbauer spectrometers (MIMOS II) on board the Mars Exploration Rovers Spirit and Opportunity, which have detected a variety of iron minerals on Mars, including magnetite ($Fe^{2+}Fe^{3+}{}_2O_4$) and goethite (α-FeO(OH)). On Earth, both minerals can derive from microbiological activity (e.g. through dissimilatory iron reduction of ferrihydrite by Fe(III)-reducing bacteria). Here we used a lab based MIMOS II to characterize the mineral products of biogenic transformations of ferrihydrite to magnetite by the Fe(III)-reducing bacteria *Geobacter sulfurreducens*. In combination with Raman spectroscopy and X-ray diffraction (XRD), we observed the formation of magnetite, goethite and siderite. We compared the material produced by biogenic transformations to abiotic samples in order to distinguish abiotic and biotic iron minerals by techniques that are or will be available onboard Martian based laboratories. The results showed the possibility to distinguish the abiotic and biotic origin of the minerals. Mossbauer was able to distinguish the biotic/abiotic magnetite with the interpretation of the geological context (Fe content mineral assemblages and accompanying minerals) and the estimation of the particle size in a non-destructive way. The Raman was able to confirm the biotic/abiotic principal peaks of the magnetite, as well as the organic principal vibration bands attributed to the bacteria. Finally, the XRD confirmed the particle size and mineralogy.

1. Introduction

The iron redox cycle is a significant process that takes place in most environments on Earth, which can be conducted by both abiotic and microbial processes. In anoxic, pH-neutral environments, microbial Fe(II)-oxidation is driven by either nitrate reducing bacteria (e.g. *Acidovorax* sp. BoFeN1), photoferrotrophic bacteria (e.g. *Rhodopseudomonas palustris* strain TIE-1) or neutrophilic microaerophilic bacteria (e.g. *Gallionella leptothrix*) (Kappler et al., 2005; Kappler and Newman, 2004; Kappler and Straub, 2005). The other half of the Fe cycle is driven by microbial Fe(III) reduction, either intracellularly by magnetotactic bacteria (Blakemore, 1975) or outside of the cell wall by dissimilatory iron reducing bacteria (DIRB) such as *Shewanella oneidensis* and *Geobacter sulfurreducens* (Lovley and Phillips, 1988, 1986). DIRB combine the oxidation of an organic substrate (e.g. acetate or lactate) or hydrogen with the reduction of poorly crystalline, short range ordered, Fe(III) minerals (e.g. ferrihydrite $(Fe^{3+})_2O_3 \bullet 0.5H_2O$) and can lead to the formation of many different iron mineral phases and compounds including goethite, magnetite, green rust and siderite ($FeCO_3$)

* Corresponding author.
E-mail address: elalla@yorku.ca (E. Lalla).

http://dx.doi.org/10.1016/j.icarus.2017.05.017
0019-1035/

(Byrne et al., 2011). The mineralogical composition of these products of reduction depends on geochemical parameters, including Fe(III) reduction rate, pH, temperature and the presence of electron shuttles (e.g. riboflavin, quinones and humic acids) (O'Loughlin et al., 2010; Piepenbrock et al., 2011). Furthermore, a recent study suggests that magnetite can act as both an electron donor and an electron acceptor to different types of Fe metabolizers depending on the redox conditions (Byrne et al., 2015). In this regard, understanding the mineralogical products of biomineralization processes can help to detect signatures of microbial interactions with fluid, rocks, mineral deposits and subsequent diagenesis.

Several terrestrial environments where microbially driven Fe(III) reduction processes occur (Léveillé, 2009; Rothschild and Mancinelli, 2001) have been identified, such as Rio Tinto (SW Spain), Western Australian salt lake sediments (SW, Australia) and Ten Graben fault system of Green River (Utah, USA), have been proposed as terrestrial analogues to the types of conditions on Mars where iron cycling could have taken place (Nixon et al., 2012; Ruecker et al., 2016). These terrestrial analog systems allude to the existence of Fe(III)-oxyhydroxide bio-signatures and fossilized microorganisms, with Fe(III)-oxyhydroxides susceptible to recrystallization to more stable forms (Léveillé, 2009; Nixon et al., 2012; Parenteau et al., 2014; Ruecker et al., 2016). Utilizing Laboratory studies and natural analogues can be used to help identify biosignatures preserved from the past (NASAś Mars Exploration Rover Mission *Spirit*), current (NASAś Mars Exploration Rover Mission *Opportunity*; Mars Science Laboratory (MSL) *Curiosity*) or future Mars missions (ESA-ExoMars rover; NASA Mars 2020) (Bish et al., 2013; Bost et al., 2015).

One of the most important techniques for characterizing Fe minerals on Mars is ^{57}Fe Mössbauer spectroscopy. This technique is capable of determining the oxidation state of iron, as well the mineralogy and the magnetic structure of different Fe mineral phases (Helgason, 2004). Indeed, two miniaturized Mössbauer spectrometers (MIMOS II) were part of the suite of analytical instruments carried on board the two Mars rovers Spirit and Opportunity, which landed on January 4, 2004 and January 25, 2004, respectively (Klingelhöfer et al., 2003). The data collected by these vehicles have provided a significant insight into the mineralogy of iron compounds on the Martian surface (Klingelhöfer et al., 2004, 2003; Morris et al., 2010, 2006, 2004). Raman and X-ray diffraction (XRD) techniques are among the payload of other current and future space missions (Bish et al., 2013; Bost et al., 2015, 2013). This includes the CheMin XRD system on the NASA MSL Curiosity mission (Bish et al., 2013) and Raman instruments such as the SHERLOC (Scanning Habitable Environment with Luminiscence for Organics and Chemical Instrument) system, the Raman SuperCam that were selected for the NASA Mars 2020 rover, and the Raman Laser Spectrometer (RLS) of the ESA ExoMars rover (Grossman, 2013; Hutchinson et al., 2014; Léveillé, 2009; Wang et al., 2015).

In this study, we investigated the formation of biogenic magnetite nanoparticles through microbial Fe(III)-reduction by the DIRB *Geobacter sulfurreducens* in the presence and absence of the electron shuttling compound Anthraquinone-2,6-disulfonate (AQDS). The presence of the electron shuttle is expected to greatly increase the speed of microbial Fe(III)-reduction compared to experiments in which it is not present. The presence/absence of AQDS should therefore have an impact on the type of mineral phases which are produced during the reduction and affect their stoichiometry (i.e. Fe(II)/Fe(III) ratio). The spectroscopic and mineralogical characteristics of these minerals were compared to those of minerals formed from abiotic syntheses in laboratory and to natural samples. The main goal of this study is to distinguish between iron minerals formed through abiotic and biotic process by techniques that are or will be available onboard Martian based laboratories. In most cases, Mössbauer spectroscopy can only be applied to dry powdered materials or embedded in a solid matrix such as in ice or on a filter. Here, however, we use the MIMOS II instrument to analyze *in situ*, a solid material that has deposited from an aqueous suspension. Our study is analogous to experiments conducted by Zegeye et al. (2010) who performed *in situ* monitoring of lepidocrocite bioreduction and magnetite formation by backscattering Mössbauer spectroscopy (Zegeye et al., 2011, 2010).

2. Experimental setup

2.1. Preparation of ^{57}Fe enriched Fe(III)- oxyhydroxide

A starting precipitate of ^{57}Fe enriched (~12%) Fe(III)-(oxyhydr)oxide was prepared to enhance the signal-to-noise ratio of the Mössbauer spectrum obtained for sediment in water. Powdered naturally abundant isotope ^{NA}Fe(0) and pure ^{57}Fe(0) were separately dissolved in 0.7 M anoxic HCl in an anoxic glovebox (MBRAUN, 100% N_2 atmosphere) and continuously stirred overnight at 400 rpm leading to the formation of $^{NA}Fe^{2+}$ and $^{57}Fe^{2+}$, respectively. The two solutions were filtered (0.22 µm syringe tip filter) to remove any solid precipitates, then mixed in a volume ratio of 10% ^{57}Fe and 90% ^{NA}Fe and removed from the glovebox. The ^{57}Fe (i.e. containing ~12% ^{57}Fe) enriched solution was oxidized using 400 µl H_2O_2 (37%) and stirred at 400 rpm for 2 hours to form an aqueous solution of acidified Fe^{3+}. KOH (5 M) was added dropwise to the Fe^{3+} solution, leading to the precipitation of the Fe(III)-oxyhydroxide, at a final pH = 7. The precipitate was washed of additional ions by centrifugation (4000 rpm, 20 min) three times, with the supernatant discarded and the precipitate re-suspended in ultrapure H_2O. After the final centrifugation step, the material was kept in liquid suspension and put into a 20 ml headspace vial. The suspension was made anoxic (but not dried) by applying vacuum (5 min) followed by flushing with N_2 gas (30s), with both steps repeated three times. The final concentration of iron in the Fe(III)-oxyhydroxide suspension was determined using the ferrozine assay (Stookey, 1970) to be 421 mmol l^{-1}.

2.2. Fe(III)-reduction experiments

Two separate experiments were carried out using the ferrihydrite at different times, with one in 2013 and the second in 2014. For both sets of experiments, *Geobacter sulfurreducens* bacteria were grown until the late log phase in basal medium (Ehrenreich and Widdel, 1994), containing 25 mM acetate (electron donor), 40 mM fumarate (electron acceptor) and buffered with 22 mM $NaHCO_3$. The bacteria were then centrifuged three times (4000 rpm; 20 min) to remove the growth medium and washed with 30 mM $NaHCO_3$ in between centrifugation steps. The final cell suspension was made up to a volume of 2 ml and the optical density at $\lambda = 600$ nm (OD_{600}) measured at 0.385 abs and 0.372 abs (FlashScan 550, Analytik Jena, Germany) for experiments in 2013 and 2014 respectively.

All Fe(III) reduction experiments were prepared in Plexiglas holders with a 500 µm bottom thickness. For 2013 experiments, cultures were prepared up to a volume of 15 ml in the glovebox using sterile, anoxic solutions and consisted of 50 mmol L^{-1} Fe(III)-(oxyhydr)oxide, 20 mM acetate and 30 mM $NaHCO_3$. One of the cultures additionally contained AQDS (10 µM) as an electron shuttle. Both culture experiments were sealed with a rubber butyl stopper to maintain an anoxic environment. The culture experiments were inoculated with 0.312 ml of *G. sulfurreducens* cell suspension immediately prior to loading on to the MIMOS II device. The cultures are subsequently referred to as FH+AQDS-13 and FH-AQDS-13.

Table 1
Mössbauer parameters of experimental and Martian samples.

Sample	Mineral phase	CS (δ) mm s^{-1}	Linewidth (S) mm s^{-1}	ΔE_Q mm s^{-1}	B_{hf} T	Relative area %	Fe(II)/Fe(III) in Fe_3O_4
FH-AQDS-14 (*in situ*, 6 h)	Ferrihydrite	0.34	0.25	0.74		100	
FH-AQDS-14 (*in situ*, 19 days)	Ferrihydrite	0.34	0.34	0.77		11.4	
	Magnetite nanophase[a]	0.33	0.24	0.53		21.7	
	Magnetite nanophase[b]	0.13	0.92	−0.03	29.5	66.9	
FH-AQDS-14 (filtered)	Ferrihydrite	0.34	0.20	0.74		0.5	
	Magnetite (tet- Fe^{3+})	0.30	0.30	0.00	48.1	40.1	
	Magnetite (oct-Fe^{2})	0.54	0.34	−0.04	44.9	21.7	
	Magnetite nanophase[b]	0.43	0.54	0.00	41.2	15.8	
	Goethite nanophase	0.39	0.35	−0.06	27.6	21.9	
FH-AQDS-13 (filtered)	Magnetite (tet-Fe^{3+})	0.30	0.19	0.00	46.6	20.8	0.65
	Magnetite (oct-Fe^{2})	0.56	0.52	−0.00	42.8	79.2	
FH+AQDS-13	Magnetite (tet-Fe^{3+})	0.33	0.40	0.00	44.0	18.6	0.25
	Magnetite (oct-Fe^{2})	0.69	0.36	0.01	42.8	12.1	
	Magnetite nanophase[b]	0.45	1.07	0.01	36.6	35.7	
	Magnetite nanophase[b]	0.71	0.59	0.04	18.0	11.4	
	Siderite	1.21	0.31	1.90		22.2	
Athena Reference Sample 043	Magnetite (tet-Fe^{3+})	0.29	0.2	0.01	49.4	37.1	0.46
	Magnetite (oct-Fe^{2})	0.66	0.2	0.00	46.1	62.9	
Average Mars magnetite[c]	Magnetite (tet-Fe^{3+})	0.31 ± 0.03		0.01 ± 0.03	50.0 ± 0.5		
	Magnetite (oct-Fe^{2})	0.66 ± 0.06		-0.01 ± 0.08	46.7 ± 0.8		
Average Mars goethite[c]	Goethite	0.38 ± 0.02		-0.19 ± 0.10	37.3 ± 2.9		

[a] Superparamagnetic magnetite - magnetic ordering prevented by small particle size.
[b] Magnetically ordered magnetite that has not reached full hyperfine splitting because of small particle size and/or impurities
[c] Values from Morris et al. (2008), averaging all magnetite and goethite measurements obtained in Gusev Crater with Mars Exploration Rover Spirit. Uncertainties quoted are standard deviations (2σ).

For the 2014 experiment, the culture were prepared in a similar way, however it contained double the concentration of iron material, i.e. 100 mmol L^{-1} Fe(III)-oxyhydroxide, 40 mM acetate and 30 mM $NaHCO_3$. There was no AQDS present. The 2014 experiment was inoculated with 0.644 ml of the *G. sulfurreducens* cell suspension, so approximately twice as many cells as for the 2013 experiment. This culture is referred hereafter as FH-AQDS-14.

2.3. Analytical methods

During the 2014 experiments, *in situ* Mössbauer measurements were carried out throughout the course of the experiment on each samples and it preparation. These *in situ* Mössbauer spectra were collected by placing the culture incubation vessels onto a MIMOS II in backscattering geometry at the Mössbauer Group of Mainz University (Germany) and left for the duration of the experiment. The culture vessels during the 2013 experiments were left on the MIMOS II, however the recorded spectra were not of sufficient quality due to their lower iron concentrations. Following the reduction phase of each experiment, the contents of each of the reaction vessels were filtered with Millipore swinnex filter holders and Millipore membrane filters (0.45 µm - HAWP04700). The entire solution of these experiments were passed through the filter and then dried under an N_2 atmosphere. Filtered samples were sealed in between two layers of Kapton tape to inhibit oxidation of the samples during measurement, and Mössbauer spectra were collected with the MIMOS II instrument. Spectra were calibrated against alpha-iron at room temperature and fitted with an in house routine (Mbfit) using Lorentzian and Voigt line profiles. Mbfit is based on the least-squares minimization routine MINUIT (James, 2004). All Mössbauer fitting parameters are shown in Table 1 (i.e. center shift (CS), quadrupole splitting (ΔE_Q), hyperfine field (B_{hf})).

Dried samples from the 2013 experiments (i.e. FH-AQDS-13 and FH+AQDS-13) were analyzed using X-ray diffraction (XRD), with data collected using a Bruker D8 Discovery Diffractometer equipped with a molybdenum $K_{\alpha 1}$ X-ray tube ($\lambda = 0.71$ Å) at the Institut für Anorganische Chemie und Analytische Chemie of Mainz University (Germany). Total scattering was measured between 5° and 40° 2θ. A comparison with a natural rock magnetite standard has been done. The natural magnetite used belongs to the NASA Athena Reference Samples (Aref 043) (Schröder, 2003). Magnetite sample was ground in an agate mortar and fixed onto a polymer tape (Scotch). The data were refined using the Rietveld method (Rietveld, 1969) and the FULLPROF software (Rodríguez-Carvajal, 1993). A pseudo-Voigt function was used to describe the peak shape and a polynomial function with five refinement coefficients for the background.

Spectroscopic Raman measurement were performed at the Unidad Asociada Uva-CSIC (Valladolid, Spain) on the dried samples from the 2013 experiments (i.e. FH-AQDS-13 and FH+AQDS-13). The Raman mineralogical characterization of the sample was performed by micro-Raman spectroscopy, using a microscope Nikon Eclipse E600 coupled to a spectrometer KOSI Holospec f/1.8i with a resolution of 5 cm^{-1} illuminated by a laser REO LSRP-3501, He-Ne 632.8 nm. The detection was performed by a CCD Andor DV420A-OE-130 with a resolution of 5 cm^{-1}. The laser power used is 14 mW with a spot diameter of 15 µm. The kapton cover of prepared samples produce strong Raman fluorescence. The material was carefully extracted from the Plexiglas holders inside a chamber/bell with a nitrogen atmosphere to avoid abiotic oxidation. Moreover, some natural iron-oxides, sulfate and carbonate from the sample collection of the ESA-ExoMars Raman Laser Spectrometer (RLS) database were measured and used as a reference materials. The reference samples stem (1) from several fieldtrips to

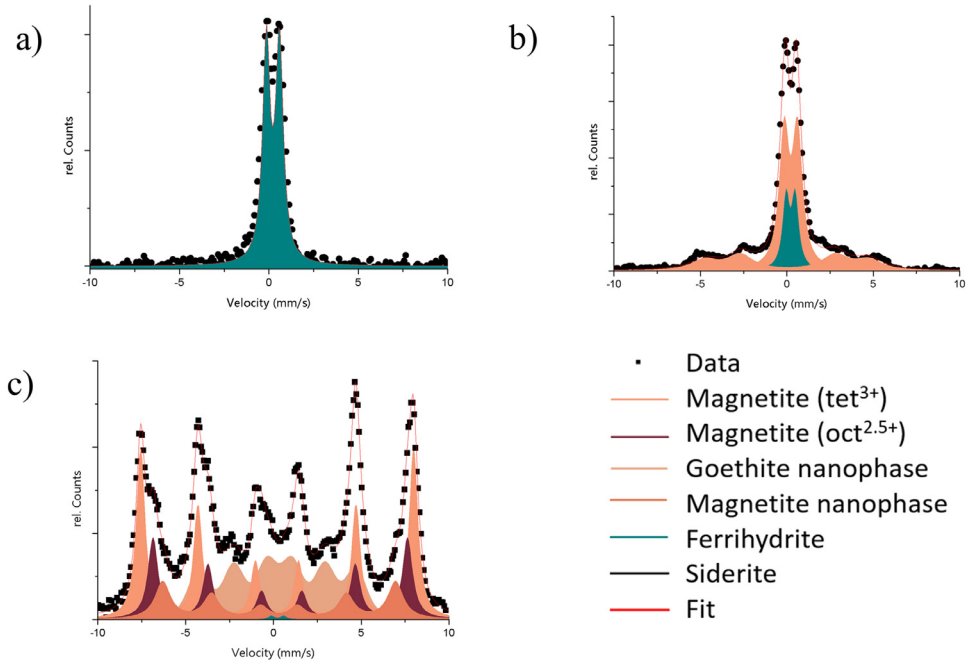

Fig. 1. MIMOS II analysis from the 2014 experiments (a) *in situ* measurement 6h after start FH-AQDS on the MIMOS II, (b) *in situ* measurement 19 days after start FH-AQDS on the MIMOS II, (c) filtered sample room temperature FH-AQDS.

terrestrial analogues including Rio Tinto (Spain), Tenerife (Spain), Svalbard (Norway), Faroe Island, etc. (Lalla et al., 2016, 2015; Sansano et al., 2015) or (2) were synthetized in the laboratory (Sansano-Caramazana, 2015). The spectral Raman collection of the mineral phases has been obtained using standard Raman systems and the RLS simulator system, processed and analyzed using the protocols for the ExoMars mission (Hermosilla et al., 2012).

3. Results

3.1. Mössbauer analysis

Data were obtained for the FH-AQDS-14 experiment which was incubated at room temperature on a MIMOS II throughout the microbial Fe(III) reduction over the course of 19 days (Fig. 1a and b) and are consequently referred to as *in situ* measurements. Fig. 1a shows the recorded spectrum obtained for FH-AQDS-14 after 6 h, with a clear doublet visible despite the fact that the starting precipitate (ferrihydrite) is suspended in liquid media. Fig. 1b shows the recorded spectrum for FH-AQDS-14 after 19 days of incubation on the MIMOS II, with the data clearly indicating the presence of both a doublet and sextet. After 19 days the microbial Fe(III) reduction in the *in situ* experiments was stopped and the precipitates were filtered. The filtered samples were then placed onto the MIMOS II again for further analysis, with Fig. 1c showing the spectrum from the FH-AQDS-14 filtered sample at room temperature. It is clear from the figure that after 6 h, the sample displays a spectrum corresponding to ferrihydrite, whilst after 19 days, the sample shows a clear sextet which likely corresponds to magnetite. After filtration (Fig. 1c), the sample displays a more characteristic spectrum of magnetite, though additional peaks corresponding to ferrihydrite and goethite appear to be present.

Fig. 2 shows the data collected for FH-AQDS-13 (Fig. 2a) and FH+AQDS-13 (Fig. 2b) experiments measured at room temperature after filtration and loaded directly onto the MIMOS II instrument. The Mössbauer spectra for a reference sample of magnetite (Athena Reference Sample 043) is shown in Fig. 2c for comparison and clearly shows the tetrahedral and octahedral lattice sites expected for the mineral. Fig. 2 indicates that ferrihydrite FH-AQDS-13 was transformed mainly into pure magnetite, whilst FH+AQDS-13 was transformed to magnetite, but with traces of siderite.

Table 2
Bands used as diagnostic for the curve fitting identification of principal iron oxide phases. The values in bold are the most intensive from each mineral.

Mineral phase	Principal Raman bands (cm^{-1})
Goethite	244, 299, **385**, 480, 681
Hematite	**225,** 245, 290–300, 412
Lepidocrocite	**250**, 348, 379, 528, 650
Siderite	184, 287, 722, **1082**
Ferrihydrite	370, 510, **710**
Magnetite	310, 540, **670**
Maghemite	350, 512, **665, 730**

3.2. XRD

XRD data shown in Fig. 3 confirms that the only mineral phase present in sample FH-AQDS-13 at the end of the experiment was magnetite whereas sample FH+AQDS-13 contained both magnetite and siderite, confirming the Mössbauer results. The structure of magnetite is centrosymmetric and shows cubic symmetry with space group *Fd-3 m*. The lattice parameter for FH-AQDS-13 and the FH+AQDS-13 samples show values around 8.30 Å which is comparable to known standards. The average crystallite sizes for both samples (also known as the coherent scattering domain) has been determined through the use of the Scherrer equation (Scherrer, 1918), being around 27–30 nm.

3.3. Raman analysis

Raman spectroscopy was carried out on selected areas of samples FH+AQDS-13 and FH-AQDS-13 (Fig. 4) and compared to reference bands for several different iron minerals (Table 2) (Hanesch, 2009). The measured data has been processed by a Gaussian curve fitting analysis on each band to obtain the

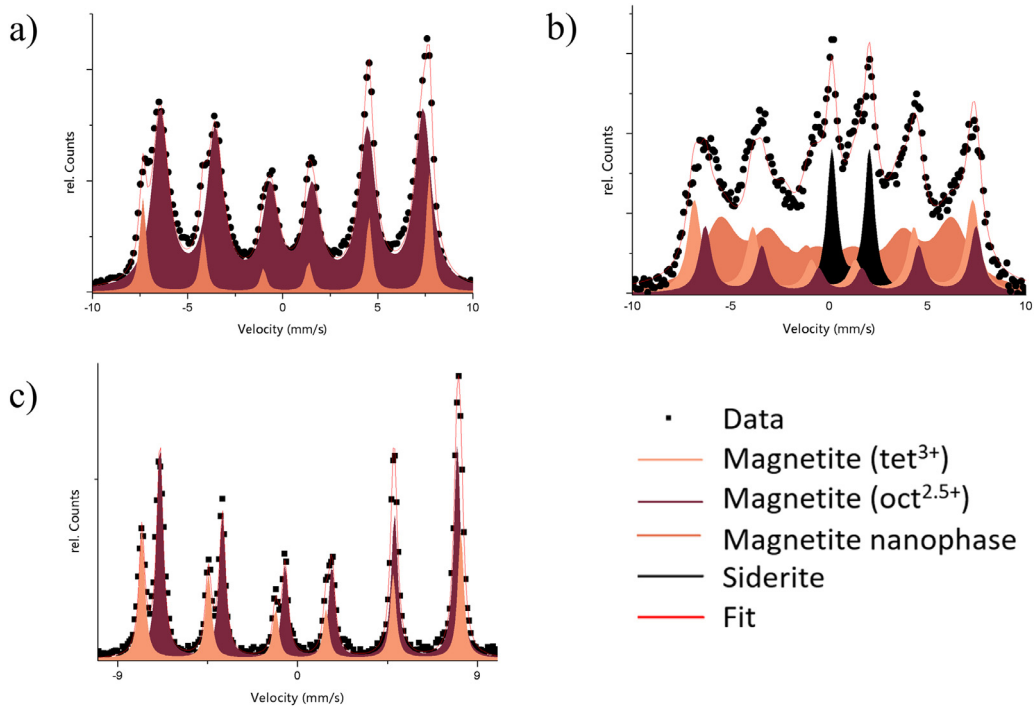

Fig. 2. MIMOS II analysis from the 2013 experiments (a) FH-AQDS measured at room temperature; (b) FH+AQDS measured at room temperature; (c) Magnetite (Athena reference sample 043).

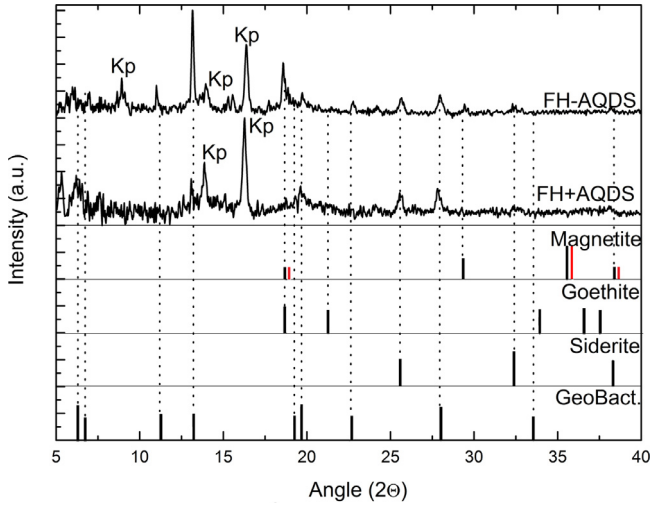

Fig. 3. XRD pattern for FH-AQDS and FH+AQDS. Samples show a broad reflection between 5° and 15° 2θ due to the Kapton film (Kp) in which they were sealed.

correct band position of the different minerals phases on the spectra. The fitting has been obtained by using the commercial program Bruker OPUS and following the standard procedure: spectra smoothing (if it is needed), background subtraction, normalization and interactive curve fitting (by Levenberg-Marquardt and/or Local Least Squares methods).

The results show the existence of several mineral oxides such as hematite, magnetite, siderite, and possibly poorly crystalline goethite in the band fitting (Fig. 4 and Table 3a). The bands in the region at 120 to 220 cm^{-1} belong unambiguously to the siderite being present on the different spectra. Secondly, the bands of the region 220–420 cm^{-1} have been assigned to the vibration of hematite (~225, ~245, ~290 cm^{-1}), siderite (~287 cm^{-1}), goethite (~244, ~300 and ~385 cm^{-1}) and magnetite (310 cm^{-1}). However, the bands corresponding to FH-AQDS-13 (Fig. 4a and 4b) are more intense compared to FH+AQDS-13 (Fig. 4c and d) due to the influence of goethite presenting the strongest vibration in this band region (according to the band fitting). On the other hand, the region 420–550 cm^{-1} presents the vibration of goethite (~480 cm^{-1}), magnetite (~530 cm^{-1}), hematite (~500 cm^{-1}) and siderite (~500 cm^{-1}). The bands on FH-AQDS-13 obtained by the curve fitting show a strong influence caused by amorphous goethite (Fig. 4a and b).

Table 3a
Raman general position in curve fitting of the Raman spectra from FH+AQDS-13 and FH-AQDS-13 samples.

Raman band position (cm^{-1})	Raman assignment
172 (w)	*****
186 (w)	Siderite
283 (m)	Hematite/Goethite/Siderite
340 (m)	Magnetite
378 (m)	Hematite/Goethite
420 (vw)	Goethite
451 (sh)	[a]
474 (m)	Goethite
495 (s)	Siderite/Magnetite
533 (sh)	Magnetite
650 (sh)	[a]
667 (vs)	Magnetite
717 (vs)	Siderite
755 (sh)	*G. sulfurreducens*
1000 (w)	*G. sulfurreducens*
1082 (w)	Siderite
1314 (m)	Hematite/Goethite
1358 (w)	*G. sulfurreducens*
1370 (w)	*G. sulfurreducens*
1422 (m)	Carbon vibration
1565 (m)	Carbon vibration
1598 (w)	*G. sulfurreducens*
2328 (w)	*G. sulfurreducens*
2903 (s)	C–H(Organics)
2961 (m)	C–H (Organics)

[a] Raman band not assigned.

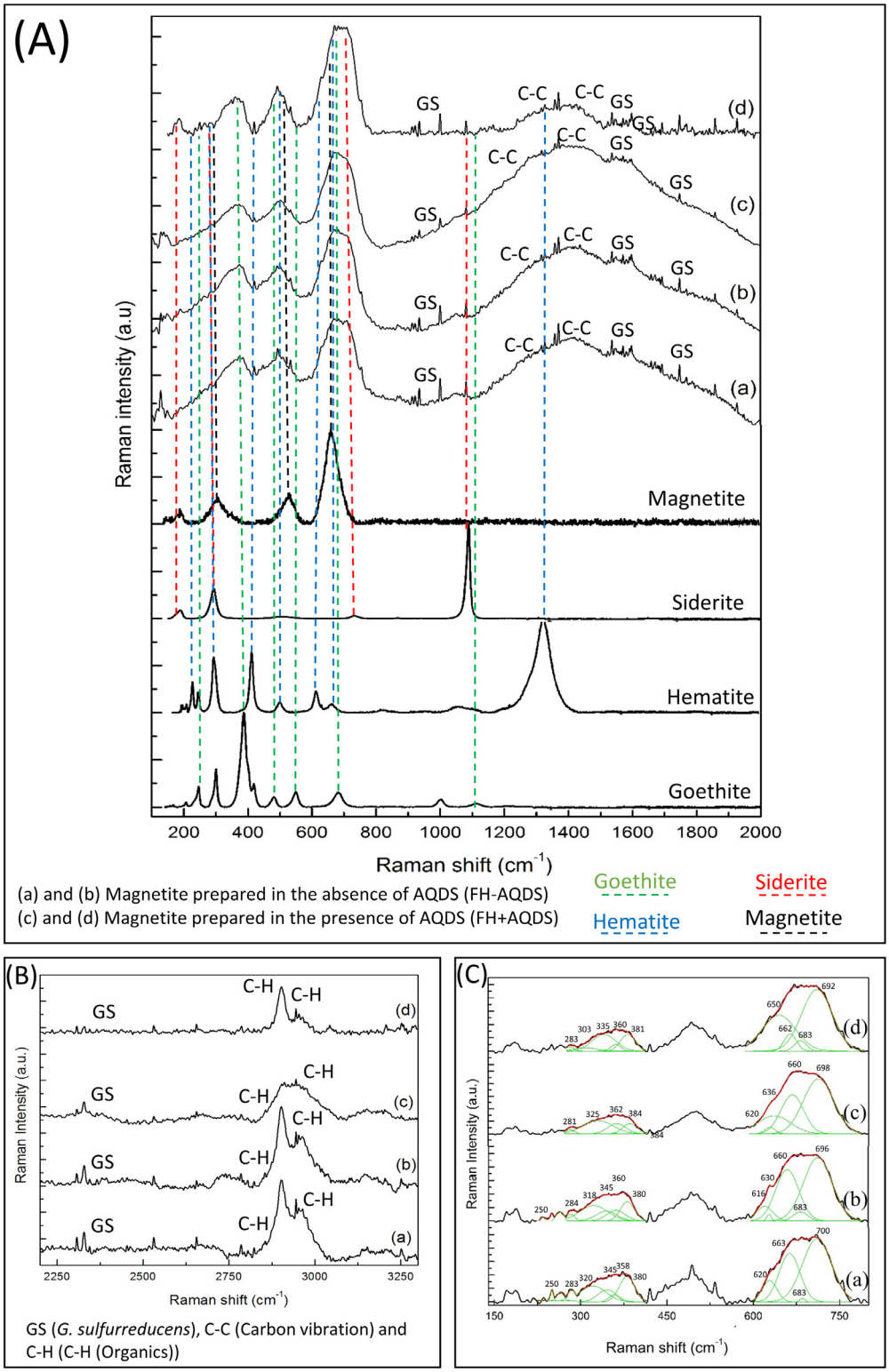

Fig. 4. (A) Raman spectra from 100 to 2000 cm^{-1} of (a) and (b) Magnetite prepared in the absence of AQDS (FH-AQDS); (c) and (d) Magnetite prepared in the presence of AQDS (FH+AQDS). Assignment of the most intense Raman vibration: Hematite, Magnetite, Goethite, Siderite, GS (G. sulfurreducens) and C–C (Carbon vibration). (B) Raman spectra from 2000 to 3000 cm^{-1} of (a) and (b) Magnetite prepared in the absence of AQDS (FH-AQDS); (c) and (d) Magnetite prepared in the presence of AQDS (FH+AQDS). Assignment of the most intense Raman vibration: C–H (C–H (Organics) and GS (G. sulfurreducens). (C) Gaussian band fitting of the regions: 200–420 cm^{-1} and 600 to 800 cm^{-1}.

The region from 560 to 800 cm^{-1} can be assigned mainly to the magnetite (~650 cm^{-1}), possibly goethite (681 cm^{-1}), hematite (~610 and ~660 cm^{-1}) and siderite (~720 cm^{-1}). Finally, the region within the 1200–1650 cm^{-1} presents a mixture of bands that belong to hematite/goethite magnon (~1350 cm^{-1}) and organics (~1314, ~1422, ~1545 and ~1575 cm^{-1}).

The magnetite bands are clearly visible at 300, 532 and 661 cm^{-1} which are in close agreement with other studies

(Hanesch, 2009; Shebanova and Lazor, 2003). The intense bands corresponding to the A_{1g} mode at 667 cm^{-1} presents a variation of magnetite measured in other studies. The A_{1g} oxide peak of magnetite is shifted toward higher wave numbers in the bio-magnetite (700 cm^{-1}) compared to that of the inorganically produced magnetite (670 cm^{-1}) (Jimenez-Lopez et al., 2010). In previous studies, it has been found that a transition to an orthorhombic phase on a starting oxidation process produces a displacement of the A_{1g} to higher values (Shebanova and Lazor, 2003). The second magnetite band between 532 and 550 cm^{-1} is reported as the mode F_{2g} and is observed to be sensitive to possible defects in the crystal structure as well as the presence of vacancies and interstitial cations. Furthermore, other studies suggest that the F_{2g} band below to 500 cm^{-1} can be attributed to the occurrence of hematite (de Faria et al., 1997; Hanesch, 2009; Shebanova and Lazor, 2003). The siderite presents the strongest band at 182, 287, 731 and 1090 cm^{-1} (Hanesch, 2009; Rull et al., 2004).

The band fitting also reveals the existence of hematite and it presents as a combination of several vibrations at 225, 245, 291, 410, 500 and 611 cm^{-1} with the magnon at 1321 cm^{-1} (Hanesch, 2009). In the case of the possible goethite presence, the principal vibrations are at 244, 299, 385, 480 and 681 cm^{-1} being the most commonly used for the identification in complex vibrational analysis (de Faria et al., 1997; Hanesch, 2009; Rull et al., 2004). The bands at the aforementioned positions are very weak and broadened, due to poorly crystallized goethite, which is combined with other oxide mineral phases (magnetite and hematite).

When considering the Raman bands of biological component, the most intense vibrations were detected between 1300 and 1600 cm^{-1}, which can be assigned to the active modes D and G of the C–C bonds vibrations from carbonaceous materials. The band fitting corresponding to this vibrational region presents several medium intensity vibrations at 1314, 1422 and 1565 cm^{-1} according to the best fitting analysis. The bands at 1314 and 1422 cm^{-1} can be assigned to the D double modes D1 and D2, which is in agreement with other studies (Ferrari, 2007). However, it has been found during band fitting that an influence of other magnon vibrations of hematite/goethite phases on 1350 cm^{-1} (Hanesch, 2009; Rull et al., 2007) is possible. The band G has also been observed (see Table 3a), showing a distorted structure clearly detectable by the broad bands. The vibrations at 2903 and 2961 cm^{-1} correspond to the C–H vibrational regions, which could be assigned to symmetric and asymmetric stretching of the $-CH_3$ from the organic matter (Böttger et al., 2012; Pereira et al., 2007). Furthermore, the *G. sulfurreducens* Raman vibration bands can be assigned to the peaks detected along the different spectra measurements. In this regard, several vibrations have been identified considering the following regions: (1) the C–H stretching region bands on 2900–3000 cm^{-1}; (2) the CH deformation vibrational region between 1300 and 1450 cm^{-1}; and (3) the C=O stretching vibration zone in 1650 to 1800 cm^{-1} approximately (el-Kabbani et al., 1991; Kudelski, 2005).

4. Discussion

The *in situ* Mössbauer spectrum for FH-AQDS-14 after 6 h is dominated by the presence of a doublet corresponding to ferrihydrite. After 19 days the sample is still dominated by a central ferric doublet, although a sextet is clearly evident. In the filtered sample however Fig. 1c), it is clear that the Mössbauer spectrum displays two sextets corresponding to ((1) tetrahedrally coordinated iron denoted $Fe^{3+}{}_{tet}$, and (2) octahedrally coordinated Fe which includes both Fe^{2+} and Fe^{3+}, often denoted $Fe^{2.5+}{}_{oct}$ with an additional goethite phase. This apparent difference in the sample before and after filtration is likely due to the nature of the MIMOS II instrument, with the *in situ* experiments only looking at the very bottom layer of the iron layer which was undergoing microbial transformation. A gradient in the reaction likely existed with most reduction taking place in the top portion of the sample where the mineral is more exposed to the solution (Dippon et al., 2015).When the sample was filtered, it was mixed and so the top fraction and bottom fraction were mixed and thus yielded the sextet as seen in Fig. 1c. The goethite phase present in the filtered sample of FH-AQDS-14 was fitted with a sextet in which the hyperfine magnetic field (B_{hf}) value (Table 1) is smaller than that of well-crystalline goethite, indicating that the goethite has very low crystallinity or consists of very small particles.

In the experiments carried out in 2013, sample FH-AQDS-13 (Fig. 2a) appears to have more well-defined sextets than sample FH+AQDS-13 (Fig. 2b). The broadened lines and additional broad sextet in these spectra can be explained by a lower degree of crystallinity possibly because of impurities in the magnetite structure, e.g. the incorporation of organic matter, and/or small particle sizes. In magnetically ordered phases, which present as sextets in Mössbauer spectra, these influences reduce the strength of the internal B_{hf}. A range of degrees of crystallinity then results in broad lines skewed towards smaller B_{hf} values. Small particle sizes, generally 30 nm or less, can additionally lead to an effect called superparamagnetism (Daniels and Rosencwaig, 1969). The particle sizes are then in the range of individual magnetic domains and random thermal movement of the particles leads to a net zero magnetic field and magnetic ordering appears to collapse, which manifests itself as a paramagnetic doublet in the Mössbauer spectrum instead of a magnetically ordered sextet (Daniels and Rosencwaig, 1969; Dezsi et al., 2008). Superparamagnetism appears to be visible in sample FH+AQDS-13 with the very broad lines in the Mössbauer spectrum (Fig. 2b) in agreement with previous studies which have shown the samples prepared in the presence of electron shuttles (e.g. AQDS) tend to be smaller in diameter than those without (Byrne et al., 2011). Furthermore, the FH+AQDS-13 sample clearly contains siderite which is likely due to the enhanced rate of microbially driven Fe(III) reduction, due to the presence of AQDS, resulting in an excess of Fe^{2+} in solution which can further react with the $CO_3{}^{2-}$ present in solution from the buffer system and lead to the precipitation of siderite (Cornell and Schwertmann, 2003; Hansel et al., 2003; Liu et al., 2009).

The parameters obtained from fitting the magnetite spectra closely correspond to the values expected for magnetite (Table 1). All of the hyperfine parameters determined are in general smaller than expected, however this is likely due to the sample exhibiting poorer magnetic ordering at room temperature than well-crystalline, stoichiometric magnetite (Fig. 2c). Neglecting potential differences in *f*-factor for the different Fe lattice positions, the stoichiometric ratio (x=Fe(II)/Fe(III)) of magnetite can be determined by comparing the relative areas of the two sextets according to the following equation (Da Costa et al., 1995; Daniels and Rosencwaig, 1969):

$$x = \frac{0.5\ Fe_{oct}^{2.5+}}{0.5\ Fe_{oct}^{2.5+} + Fe_{tet}^{3+}} \quad (1)$$

Using Eq. (1) it is seen that magnetite formed in FH+AQDS-13 (x = 0.25) is more oxidized than perfectly stoichiometric magnetite (x = 0.5). The iron in magnetite formed in FH-AQDS-13 (x = 0.65) is more reduced than stoichiometric magnetite. The difference is thought to be due to the faster reduction rate in the presence of AQDS, leading to the formation of superparamagnetic magnetite nanoparticles. However, this result also suggests that the presence of electron shuttles might in fact lead to the formation of rather oxidized magnetite. Since electron shuttles such as AQDS are organic compound, it might indicate that magnetite found in regions with low stoichiometry can be linked to the presence of organic substance. The relative ratio of Fe(II)/Fe(III) in the magnetite in

Table 3b
Raman Curve analysis per spectra corresponding to Fig. 3 and its possible mineral assignments compared to standards. The values in bold are the most intensive from each mineral

Mineral phase	Principal Raman fitting bands (cm^{-1}) of the mineral and organics detected			
	Raman spectra (a)	Raman spectra (b)	Raman spectra (c)	Raman spectra (d)
Goethite	283, **376**, 420, 475	284, **373**, 471	285, **383**, 420	283, **385**, 420, 480
Hematite	**250**, 283, 493, 609, 1348	**250**, 283, 401, 497, 609, 1337	**250**, 283, 403, 480, 1358	**250**, 283, 491, 609, 1331
Siderite	**187**, 505, 711, **1083**	**188**, 504, 703, **1083**	**187**, 700, **1083**	**184**, 712, **1083**
Magnetite	308, 533, **653** or **691** *(bio-mag)*[a]	315, 534, **652** or **679** *(bio-mag)*[a]	308, 534, **642** or **685** *(bio-mag)*[a]	315, 533, **652** or **690** *(bio-mag)*[a]
Organics	1327, **1370**, 1400, 1537,**1598**, 2328, 2344, 2884, **2902, 2963**	1279, **1386**, 1431, 1549, **1598**, 2307, 2328, 2874, 2902, **2963**	**1287**, 1427, 1559, **1600**, 2328, 2878, **2905**, 2940, 2974	1270, **1401**,1438, 1469, 1542, **1597**, 2874, **2903**, 2947, **2969**, 3043

[a] Refers to the magnetite produced by G. sulfurreducens. The curve fitting relative band intensity of I685-90/I650 shows for: (a) ~1.50, (b) 1.27, (c) 1.63, (d) 1.2.

FH-AQDS-13 is calculated to be higher than those previously reported and showing a higher concentration of ferrous magnetite (Veeramani et al., 2011). Moreover, the mineral phases measured are in agreement with Veeramani et al., (Veeramani et al., 2011), though here we have also identified the presence of siderite.

The XRD results for our samples show smaller values for the lattice constant(8.30 Å) than the 8.397 Å associated with stoichiometric magnetite (ICDD, n.d.; Magnetite - www.mindat.org 2001). Maghemite has a smaller lattice constant of 8.33 Å, which is more similar to our results, suggesting the samples to be partially oxidized which agrees with the Mössbauer results for sample FH+AQDS (Wohlfarth and Arrott, 1982). It has also been seen that the lattice parameters of pure and metal-substituted bio-magnetites tend to be smaller compared to those of chem-magnetites where the bio-magnetite likely has a relatively more compact crystal structure with fewer uncoordinated iron ions on the surface (Moon et al., 2010). The average crystal size is around 27–30 nm for the FH+AQDS-13 and FH-AQDS-13, being consistent with the Mössbauer observations of smaller B_{hf} values, broadened and skewed lines, and superparamagnetism. Also, this result confirms the interpretation of other studies (Byrne et al., 2011; Veeramani et al., 2011).

In the Raman results, the variation of A_{1g} mode corresponding to the magnetite could becaused by the curve fitting or may be due to structural changes generated during the microbial Fe(III) reduction where the oxidation process produces a displacement of the A_{1g} to higher values. An estimation can be done by curve fitting relative band intensity of $I_{685\text{-}90}/I_{650}$ produced by the magnetite and the bio-magnetite, the results show the existence of two Raman bands where the $I_{685\text{-}90}$ is more intense (See Table 3b and Fig. 3). Also, the FH-AQDS-13 presents the possible existence of goethite due to the higher intensity of the bands in the region between 220–420. Furthermore, it can be affirmed by the $I_{220\text{-}520}/I_{560\text{-}800}$, which for FH-AQDS-13 is at approximately 0.5 and FH+AQDS-13 is 0.35 (Fig. 3).

In the region from 2800 to 3100 cm^{-1}, the FH-AQDS-13 bands are more intense compared to those of FH+AQDS-13 spectra and confirm that the *G. sulfurreducens* transformed the starting material.

In general, the combination of Mössbauer, Raman and XRD technique allowed the detection of several iron mineral phases and mineral structures. The magnetite was the main mineral that formed as a result of microbial Fe(III) reduction by *G. sulfurreducens*. The Raman based vibrational technique was able to detect hematite with the possibility of minor phases of goethite, clearly distinguishable by the main vibrations and the curve-fitting. Mössbauer spectra indicate oxidized magnetite in the FH+AQDS-13 samples. Oxidation of magnetite leads to maghemite and eventually hematite formation, but these phases are difficult to differentiate (Vandenberghe et al., 2000).

The combination of siderite, magnetite, hematite and non-crystalline goethite suggests a relatively complex mineralization process that is strongly dependent on biological mechanism. Similar formations of mixed minerals can be achieved by chemical processes, however they often present with other phase combinations including ferrihydrite-goethite-lepidocrocite-magnetite (Hansel et al., 2005) or goethite-hematite-maghemite-magnetite-akaganeite (Ahn et al., 2012). Furthermore, the starting conditions of microbial Fe(III) reduction, such as the use of different starting substrates including hydrous ferric oxide, goethite, hematite, magnetite, carbonates, and Fe(III)-clays, or the variation of geochemical parameters including Eh, pH, and temperature can yield stark differences in the types of minerals produced via primary or secondary mineralization pathways (Jimenez-Lopez et al., 2010; Perez-Gonzalez et al., 2010).

Here we suggest that the use of Mössbauer-Raman-XRD analyses in combination with other structural studies could potentially be used to obtain a suitable range of criteria to help develop fingerprints to distinguish biological and abiotic magnetite. The biogenic magnetite and goethite from our experiments differs significantly from the magnetite and goethite observed with the Mars Exploration Rovers in rocks and soils on Mars (Table 1), where the magnetite is suggested to be of primary, igneous origin (Morris et al., 2008).

Our biogenic magnetite is non-stoichiometric and, in the case of FH+AQDS-13 appears to be oxidized. The broad lines reflect in Mössbauer spectra reflect low crystallinity, potentially resulting from impurities such as organic matter, and/or small particle sizes. The presence of organic matter is confirmed by Raman spectroscopy and small particle sizes are indicated by XRD. Taken together, the evidence extracted from the different techniques could be used to establish some criteria for bio-signatures. Table 4 presents a resume of the main features of each technique that could be used for the detection of bio-signatures in planetary exploration.

The question, however, is whether the features observed here would be preserved over geological timescales. Over time, magnetite might mature and increase in crystallinity while organic matter can undergo decay, thus potentially eliminating any evidence over extended timescales.

5. Conclusions

The MIMOS II instrument, of which two have previously been sent to Mars onboard Martian rovers, has been used to characterize different mineral phases produced by the microbial reduction of Fe(III)-oxyhydroxide and determined the dominant phase produced to be magnetite. Other techniques on current or future Mars rover missions such as XRD and Raman have been used to complement these results. Mössbauer, XRD, and Raman confirm the existence of magnetite for the samples incubated with only ferrihydrite (FH+AQDS-13 and FH-AQDS-13) and magnetite combined with siderite for the sample incubated with an added electron shuttle (FH+AQDS-13). The values of the crystal lattice show values under 8.397 Å and crystalline sizes under 30 nm being in the range of superparamagnetism as confirmed by the Mössbauer analysis.

Table 4
Comparison of the main features of Mössbauer, XRD, and Raman that can be used for potential bio-mineral detection.

Technique	Structure and crystallinity	Particle size	Detection of organics	Oxidation states	Stoichiometry	[b]Geological context
Raman spectroscopy	Yes	No	Yes	No	Potentially	Yes
XRD	Yes	Yes	No	No	No	Potentially
Mössbauer Spectroscopy[a]	Yes	Yes	No	Fe	Yes	Yes

[a] Mössbauer spectroscopy is limited to Fe-bearing materials.
[b] Geological Context: Mineral assemblages and accompanying minerals.

Raman analysis shows the formation of different mineralization products, including goethite (possibly), hematite, magnetite and siderite which is only somewhat in agreement with the Mössbauer analyses that did not observe hematite in samples. Some differences between the bio-magnetite and natural magnetite have been detected by Raman spectroscopy on the bands at approximately 650 and 540 cm^{-1}. In all spectra recorded, organic compounds were detected which correspond to the DIRB *G. sulfurreducens*.

The combination of these three different analytical techniques could be used as a critical approach for observing the products of Fe-biomineralization processes on future space missions, especially those focused on Mars. In this regard, these techniques, used in combination with morphological studies, will help to establish a criterion of the biological origin of biogenic magnetite and other Fe minerals.

Acknowledgments

The work was supported by the MICINN with the Project AYA-2008-04529 for the development of the Raman-LIBS combined spectrometer for the ESA-ExoMars Mission. C. S. acknowledges a joint postdoctoral appointment at the Universities of Bayreuth and Tübingen funded through the DFG research unit FOR 580 – electron transfer processes in anoxic aquifers (e-TraP) and an Impact Fellowship awarded by the University of Stirling. Finally, the authors would like to thank the anonymous reviewers for their helpful and constructive comments that greatly contributed to improving the final version of the paper.

References

Ahn, T., Kim, J.H., Yang, H.M., Lee, J.W., Kim, J.D., 2012. Formation pathways of magnetite nanoparticles by coprecipitation method. J. Phys. Chem. C 116, 6069–6076. doi:10.1021/jp211843g.

Bish, D.L., Blake, D.F., Vaniman, D.T., Chipera, S.J., Morris, R.V, Ming, D.W., Treiman, A.H., Sarrazin, P., Morrison, S.M., Downs, R.T., Achilles, C.N., Yen, A.S., Bristow, T.F., Crisp, J.A., Morookian, J.M., Farmer, J.D., Rampe, E.B., Stolper, E.M., Spanovich, N., Team, M.S.L.S., 2013. X-ray diffraction results from mars science laboratory: mineralogy of rocknest at gale crater. Science 341. doi:10.1126/science.1238932.

Blakemore, R., 1975. Magnetotactic bacteria. Science 190, 377–379. doi:10.1126/science.170679.

Bost, N., Ramboz, C., LeBreton, N., Foucher, F., Lopez-Reyes, G., De Angelis, S., Josset, M., Venegas, G., Sanz-Arranz, A., Rull, F., Medina, J., Josset, J.-L., Souchon, A., Ammannito, E., De Sanctis, M.C., Di Iorio, T., Carli, C., Vago, J.L., Westall, F., 2015. Testing the ability of the ExoMars 2018 payload to document geological context and potential habitability on Mars. Planet. Space Sci. 108, 87–97. doi:10.1016/j.pss.2015.01.006.

Bost, N., Westall, F., Ramboz, C., Foucher, F., Pullan, D., Meunier, A., Petit, S., Fleischer, I., Klingelhöfer, G., Vago, J.L., 2013. Missions to mars: characterisation of mars analogue rocks for the international space analogue rockstore (ISAR). Planet. Space Sci. 82–83, 113–127. http://dx.doi.org/10.1016/j.pss.2013.04.006.

Böttger, U., de Vera, J.-P., Fritz, J., Weber, I., Hübers, H.-W., Schulze-Makuch, D., 2012. Optimizing the detection of carotene in cyanobacteria in a martian regolith analogue with a Raman spectrometer for the ExoMars mission. Planet. Space Sci. 60, 356–362. http://dx.doi.org/10.1016/j.pss.2011.10.017.

Byrne, J.M., Klueglein, N., Pearce, C., Rosso, K.M., Appel, E., Kappler, A., 2015. Redox cycling of Fe(II) and Fe(III) in magnetite by Fe-metabolizing bacteria. Science 347 (80), 1473–1476. doi:10.1126/science.aaa4834.

Byrne, J.M., Telling, N.D., Coker, V.S., Pattrick, R.A.D., van der Laan, G., Arenholz, E., Tuna, F., Lloyd, J.R., 2011. Control of nanoparticle size, reactivity and magnetic properties during the bioproduction of magnetite by Geobacter sulfurreducens. Nanotechnology 22, 455709.

Cornell, R.M., Schwertmann, U., 2003. The Iron Oxides: Structure, Properties, Reactions, Occurences and Uses. Wiley-Vch p. ISBN: 3-527-30274-3 doi:10.1002/3527602097.

Da Costa, G.M., De Grave, E., De Bakker, P.M.A., Vandenberghe, R.E., 1995. Influence of nonstoichiometry and the presence of maghemite on the Mössbauer spectrum of magnetite. Clays Clay Miner 43, 656–668.

Daniels, J.M., Rosencwaig, A., 1969. Mössbauer spectroscopy of stoichiometric and non-stoichiometric magnetite. J. Phys. Chem. Solids 30, 1561–1571. doi:10.1016/0022-3697(69)90217-0.

de Faria, D.L.A., Silva, S.V., de Oliveira, M.T., 1997. Raman microspectroscopy of some iron oxides and oxyhydroxides. J. Raman Spectrosc. 28, 873–878.

Dezsi, I., Fetzer, C., Gombköt, Á., Szucs, I., Gubicza, J., Ungár, T., 2008. Phase transition in nanomagnetite. J. Appl. Phys. 103, 1–5. doi:10.1063/1.2937252.

Dippon, U., Schmidt, C., Behrens, S., Kappler, A., Dippon, U.R.S., Schmidt, C., Behrens, S., Kappler, A., 2015. Secondary mineral formation during ferrihydrite reduction by shewanella oneidensis MR-1 depends on incubation vessel orientation and resulting gradients of cells, Fe and Fe minerals. Geomicrobiol. J. 451. doi:10.1080/01490451.2015.1017623.

Ehrenreich, A., Widdel, F., 1994. Anaerobic oxidation of ferrous iron by purple bacteria, a new type of phototrophic metabolism. Appl. Environ. Microbiol. 60, 4517–4526.

el-Kabbani, O., Chang, C.H., Tiede, D., Norris, J., Schiffer, M., 1991. Comparison of reaction centers from Rhodobacter sphaeroides and Rhodopseudomonas viridis: overall architecture and protein-pigment interactions. Biochemistry 30, 5361–5369.

Ferrari, A.C., 2007. Raman spectroscopy of graphene and graphite: disorder, electron-phonon coupling, doping and nonadiabatic effects. Solid State Commun 143, 47–57.

Grossman, L., 2013. NASA urged to seek live Martians with 2020 rover. New Sci 219 (9). doi:10.1016/S0262-4079(13)61775-3.

Hanesch, M., 2009. Raman spectroscopy of iron oxides and (oxy)hydroxides at low laser power and possible applications in environmental magnetic studies. Geophys. J. Int. 177, 941–948. doi:10.1111/j.1365-246X.2009.04122.x.

Hansel, C.M., Benner, S.G., Fendorf, S., 2005. Competing Fe (II)-induced mineralization pathways of ferrihydrite. Environ. Sci. Technol. 39, 7147–7153. doi:10.1021/es050666z.

Hansel, C.M., Benner, S.G., Neiss, J., Dohnalkova, A., Kukkadapu, R.K., Fendorf, S., 2003. Secondary mineralization pathways induced by dissimilatory iron reduction of ferrihydrite under advective flow. Geochim. Cosmochim. Acta 67, 2977–2992.

Helgason, O., 2004. Processes in geophysics studied by Mossbauer spectroscopy. Hyperfine Interact. 156, 379–388. doi:10.1023/B:HYPE.0000043257.28606.14.

Hermosilla, I., Lopez-Reyes, G., Catala, A., Sanz, A., Llanos, D.R., Rull, F., 2012. Raman spectra processing algorithms and database for RLS-ExoMars. Proc. Eur. Planet. Sci. Congr. 7, 23–28.

Hutchinson, I.B., Parnell, J., Edwards, H.G.M., Jehlicka, J., Marshall, C.P., Harris, L.V, Ingley, R., 2014. Potential for analysis of carbonaceous matter on Mars using Raman spectroscopy. Planet. Space Sci. http://dx.doi.org/10.1016/j.pss.2014.07.006.

International Centre for Diffraction Data (ICDD), n.d. PDF-2 database. http://www.icdd.com/

James, F., 2004. MINUIT tutorial, function minimization, in: CERN computing and data processing school. Pertisau 10–24.

Jimenez-Lopez, C., Romanek, C.S., Bazylinski, D.A., 2010. Magnetite as a prokaryotic biomarker: a review. J. Geophys. Res. 115 (G00G03). doi:10.1029/2009JG001152.

Kappler, A., Newman, D.K., 2004. Formation of Fe(III)-minerals by Fe(II)-oxidizing photoautotrophic bacteria. Geochim. Cosmochim. Acta 68, 1217–1226. doi:10.1016/j.gca.2003.09.006.

Kappler, A., Schink, B., Newman, D.K., 2005. Fe(III) mineral formation and cell encrustation by the nitrate-dependent Fe(II)-oxidizer strain BoFeN1. Geobiology 3, 235–245. doi:10.1111/j.1472-4669.2006.00056.x.

Kappler, A., Straub, K.L., 2005. Geomicrobiological cycling of iron. Rev. Mineral. Geochem. 59, 85–108. doi:10.2138/rmg.2005.59.5.

Klingelhöfer, G., Morris, R.V, Bernhardt, B., Rodionov, D., de Souza, P.A., Squyres, S.W., Foh, J., Kankeleit, E., Bonnes, U., Gellert, R., Schröder, C., Linkin, S., Evlanov, E., Zubkov, B., Prilutski, O., 2003. Athena MIMOS II Mössbauer spectrometer investigation. J. Geophys. Res. Planets doi:10.1029/2003JE002138, 108, n/a–n/a.

Klingelhöfer, G., Morris, R.V, Bernhardt, B., Schröder, C., Rodionov, D.S., de Souza, P.A., Yen, A., Gellert, R., Evlanov, E.N., Zubkov, B., Foh, J., Bonnes, U., Kankeleit, E., Gütlich, P., Ming, D.W., Renz, F., Wdowiak, T., Squyres, S.W., Arvidson, R.E., 2004. Jarosite and hematite at meridiani planum from opportunity's Mössbauer spectrometer. Sci 306, 1740–1745. doi:10.1126/science.1104653.

Kudelski, A., 2005. Characterization of thiolate-based mono- and bilayers by vibrational spectroscopy: a review. Vib. Spectrosc.

Lalla, E.A., López-Reyes, G., Sansano, A., Sanz-Arranz, A., Schmanke, D., Klingelhöfer, G., Medina-García, J., Martínez-Frías, J., Rull-Pérez, F., 2015. Estudio espectroscópico y DRX de afloramientos terrestres volcánicos en la isla de Tenerife como posibles análogos de la geología marciana. Estud. Geológicos 71, 1–19. doi:10.3989/egeol.41927.354.

Lalla, E.A., Sanz-Arranz, A., Lopez-Reyes, G., Sansano, A., Medina, J., Schmanke, D., Klingelhoefer, G., Rodríguez-Losada, J.A., Martínez-Frías, J., Rull, F., 2016. Raman–Mössbauer–XRD studies of selected samples from "Los Azulejos" outcrop: a possible analogue for assessing the alteration processes on Mars. Adv. Sp. Res. 57, 2385–2395. doi:10.1016/j.asr.2016.03.014.

Léveillé, R., 2009. Validation of astrobiology technologies and instrument operations in terrestrial analogue environments. Comptes Rendus Palevol 8, 637–648. http://dx.doi.org/10.1016/j.crpv.2009.03.005.

Liu, H., Li, P., Lu, B., Wei, Y., Sun, Y., 2009. Transformation of ferrihydrite in the presence or absence of trace Fe(II): The effect of preparation procedures of ferrihydrite. J. Solid State Chem. 182, 1767–1771.

Lovley, D.R., Phillips, E.J.P., 1988. Novel mode of microbial energy metabolism: organic carbon oxidation coupled to dissimilatory reduction of iron or manganese. Appl. Envir. Microbiol. 54, 1472–1480.

Lovley, D.R., Phillips, E.J.P., 1986. Availability of Ferric iron for microbial reduction in bottom sediments of the freshwater tidal potomac river. Appl. Envir. Microbiol. 52, 751–757.

Magnetite - www.mindat.org [WWW Document] URL, http://www.mindat.org/min-2538.html, 2001.

Moon, J.-W., Rawn, C.J., Rondinone, A.J., Wang, W., Vali, H., Yeary, L.W., Love, L.J., Kirkham, M.J., Gu, B., Phelps, T.J., 2010. Crystallite Sizes and Lattice Parameters of nano-biomagnetite particles. J. Nanosci. Nanotechnol. 10, 8298–8306.

Morris, R.V., Klingelhöfer, G., Schröer, C., Fleischer, I., Ming, D.W., Yen, A.S., Gellert, R., Arvidson, R.E., Rodionov, D.S., Crumpler, L.S., Clark, B.C., Cohen, B.A., McCoy, T.J., Mittlefehldt, D.W., Schmidt, M.E., De Souza, J.A., Squyres, S.W., 2008. Iron mineralogy and aqueous alteration from husband hill through home plate at gusev crater, mars: results from the mössbauer instrument on the spirit mars exploration rover. J. Geophys. Res. E Planets 113.

Morris, R.V., Klingelhöfer, G., Bernhardt, B., Schröder, C., Rodionov, D.S., de Souza, P.A., Yen, A., Gellert, R., Evlanov, E.N., Foh, J., Kankeleit, E., Gütlich, P., Ming, D.W., Renz, F., Wdowiak, T., Squyres, S.W., Arvidson, R.E., 2004. Mineralogy at gusev crater from the mössbauer spectrometer on the spirit rover. Science 305 (80), 833–836 LP.

Morris, R.V., Klingelhöfer, G., Schröder, C., Rodionov, D.S., Yen, A., Ming, D.W., de Souza, P.A., Fleischer, I., Wdowiak, T., Gellert, R., Bernhardt, B., Evlanov, E.N., Zubkov, B., Foh, J., Bonnes, U., Kankeleit, E., Gütlich, P., Renz, F., Squyres, S.W., Arvidson, R.E., 2006. Mössbauer mineralogy of rock, soil, and dust at gusev crater, mars: spirit's journey through weakly altered olivine basalt on the plains and pervasively altered basalt in the columbia hills. J. Geophys. Res. Planets 111. doi:10.1029/2005JE002584, n/a–n/a.

Morris, R.V, Ruff, S.W., Gellert, R., Ming, D.W., Arvidson, R.E., Clark, B.C., Golden, D.C., Siebach, K., Klingelhöfer, G., Schröder, C., Fleischer, I., Yen, A.S., Squyres, S.W., 2010. Identification of carbonate-rich outcrops on mars by the spirit rover. Science 329, 421–424. doi:10.1126/science.1189667.

Nixon, S.L., Cockell, C.S., Tranter, M., 2012. Limitations to a microbial iron cycle on Mars. Planet. Space Sci. 72, 116–128. doi:10.1016/j.pss.2012.04.003.

O'Loughlin, E.J., Gorski, C.A., Scherer, M.M., Boyanov, M.I., Kemner, K.M., 2010. Effects of oxyanions, natural organic matter, and bacterial cell numbers on the bioreduction of lepidocrocite (γ-FeOOH) and the formation of secondary mineralization products. Environ. Sci. Technol. 44, 4570–4576. doi:10.1021/es100294w.

Parenteau, M.N., Jahnke, L.L., Farmer, J.D., Cady, S.L., 2014. Production and early preservation of lipid biomarkers in iron hot springs. Astrobiology 14, 502–521. doi:10.1089/ast.2013.1122.

Pereira, B.G., Vianna-Soares, C.D., Righi, A., Pinheiro, M.V.B., Flores, M.Z.S., Bezerra, E.M., Freire, V.N., Lemos, V., Caetano, E.W.S., Cavada, B.S., 2007. Identification of lamivudine conformers by Raman scattering measurements and quantum chemical calculations. J. Pharm. Biomed. Anal 43, 1885–1889.

Perez-Gonzalez, T., Jimenez-Lopez, C., Neal, A.L., Rull-Perez, F., Rodriguez-Navarro, A., Fernandez-Vivas, A., Iañez-Pareja, E., 2010. Magnetite biomineralization induced by Shewanella oneidensis. Geochim. Cosmochim. Acta 74, 967–979. doi:10.1016/j.gca.2009.10.035.

Piepenbrock, A., Dippon, U., Porsch, K., Appel, E., Kappler, A., 2011. Dependence of microbial magnetite formation on humic substance and ferrihydrite concentrations. Geochim. Cosmochim. Acta 75, 6844–6858. doi:10.1016/j.gca.2011.09.007.

Rietveld, H.M., 1969. A profile refinement method for nuclear and magnetic structures. J. Appl. Crystallogr. 2, 65–71. doi:10.1107/S0021889869006558.

Rodríguez-Carvajal, J., 1993. Recent advances in magnetic structure determination by neutron powder diffraction. Phys. B Condens. Matter 192, 55–69. http://dx.doi.org/10.1016/0921-4526(93)90108-I.

Rothschild, L.J., Mancinelli, R.L., 2001. Life in extreme environments. Nature 409, 1092–1101.

Ruecker, A., Schröder, C., Byrne, J., Weigold, P., Behrens, S., Kappler, A., 2016. Geochemistry and mineralogy of western australian salt lake sediments: implications for meridiani planum on Mars. Astrobiology 16, 525–538. doi:10.1089/ast.2015.1429.

Rull, F., Martinez-Frias, J., Rodríguez-Losada, J.A., 2007. Micro-Raman spectroscopic study of El Gasco pumice, western Spain. J. Raman Spectrosc. 38, 239–244. doi:10.1002/jrs.1628.

Rull, F., Martinez-Frias, J., Sansano, A., Medina, J., Edwards, H.G.M., 2004. Comparative micro-Raman study of the Nakhla and Vaca Muerta meteorites. J. Raman Spectrosc. 35, 497–503. doi:10.1002/jrs.1177.

Sansano-Caramazana, A., 2015. Síntesis y caracterización espectroscópica de sulfatos de hierro: implicaciones en astrobiología y la exploración de Marte. University of Valladolid.

Sansano, A., Navarro, R.J., Manrique, J.A., Medina, J., Rull, F., 2015. Multispectral analysis of Mars analog altered volcanic materials from faroe islands. Implicatons for Missions as ExoMars and Mars 2020. Lunar Planet. Sci. Conf.

Scherrer, P., 1918. Bestimmung der Grösse und der inneren Struktur von Kolloidteilchen mittels Röntgenstrahlen. Nachrichten von der Gesellschaft der Wissenschaften zu Göttingen, Math. Klasse 1918, 98–100. doi:10.1007/978-3-662-33915-2.

Schröder, C., 2003. ATHENA reference samples. Mainz.

Shebanova, O.N., Lazor, P., 2003. Raman spectroscopic study of magnetite (FeFe2O4): a new assignment for the vibrational spectrum. J. Solid State Chem. 174, 424–430. doi:10.1016/S0022-4596(03)00294-9.

Stookey, L.L., 1970. Ferrozine–a new spectrophotometric reagent for iron. Anal. Chem. 42, 779–781.

Vandenberghe, R.E., Barrero, C.A., da Costa, G.M., Van San, E., De Grave, E., 2000. Mössbauer characterization of iron oxides and (oxy)hydroxides: the present state of the art. Hyperfine Interact 126, 247–259. doi:10.1023/A:1012603603203.

Veeramani, H., Alessi, D.S., Suvorova, E.I., Lezama-Pacheco, J.S., Stubbs, J.E., Sharp, J.O., Dippon, U., Kappler, A., Bargar, J.R., Bernier-Latmani, R., 2011. Products of abiotic U(VI) reduction by biogenic magnetite and vivianite. Geochim. Cosmochim. Acta 75, 2512–2528. doi:10.1016/j.gca.2011.02.024.

Wang, A., Korotev, R.L., Jolliff, B.L., Ling, Z., 2015. Raman imaging of extraterrestrial materials. Planet. Space Sci. 112, 23–34. doi:10.1016/j.pss.2014.10.005.

Wohlfarth, E.P., Arrott, A.S., 1982. Ferromagnetic materials: a handbook on the properties of magnetically ordered substances vol. 1, 2. doi:10.1063/1.2914974.

Zegeye, A., Abdelmoula, M., Usman, M., Hanna, K., Ruby, C., 2011. In situ monitoring of lepidocrocite bioreduction and magnetite formation by reflection Mössbauer spectroscopy. Am. Mineral. 96, 1410–1413. doi:10.2138/am.2011.3794.

Zegeye, A., Mustin, C., Jorand, F., 2010. Bacterial and iron oxide aggregates mediate secondary iron mineral formation: green rust versus magnetite. Geobiology 8, 209–222. doi:10.1111/j.1472-4669.2010.00238.x.